Experimental tests of the gravitational inverse-square law for mass separations from 2 to 105 cm

J. K. Hoskins,* R. D. Newman, R. Spero,† and J. Schultz
Department of Physics, University of California, Irvine, California 92717
(Received 23 July 1985)

We report two experiments which test the inverse-square distance dependence of the Newtonian gravitational force law. One experiment uses a torsion balance consisting of a 60-cm-long copper bar suspended at its midpoint by a tungsten wire, to compare the torque produced by copper masses 105 cm from the balance axis with the torque produced by a copper mass 5 cm from the side of the balance bar, near its end. Defining $R_{\rm expt}$ to be the measured ratio of the torques due to the masses at 105 cm and 5 cm, and $R_{\rm Newton}$ to be the corresponding ratio computed assuming an inverse-square force law, we find $\delta\equiv(R_{\rm expt}/R_{\rm Newton}-1)=(1.2\pm7)\times10^{-4}$. Assuming a force deviating from an inverse-square distance dependence by a factor $[1+\epsilon\ln r(\text{cm})]$, this result implies $\epsilon=(0.5\pm2.7)\times10^{-4}$. An earlier experiment, which has been reported previously, is described here in detail. This experiment tested the inverse-square law over a distance range of approximately 2 to 5 cm, by probing the gravitational field inside a steel mass tube using a copper test mass suspended from the end of a torsion balance bar. This experiment yielded a value for the parameter ϵ defined above: $\epsilon=(1\pm7)\times10^{-5}$. The results of both of these experiments are in good agreement with the Newtonian prediction. Limits on the strength and range of a Yukawa potential term superimposed on the Newtonian gravitational potential are discussed.

I. INTRODUCTION

The possibility of a deviation of the effective gravitational force from an inverse-square distance dependence on a laboratory distance scale has received much attention in the last decade. On the experimental side this interest has been stimulated by Long's report[1] of an experiment indicating that the ratio of the gravitational force at 30 cm to that at 4.5 cm exceeds the Newtonian prediction by $(0.37\pm0.07)\%$, and by Stacey's report[2] that the value of the gravitational constant G inferred from measurements of Earth's gravitational field g as a function of depth in mine shafts, boreholes, and in the ocean is significantly higher than the laboratory value. Further, several authors[3–5] have argued that other existing laboratory, geophysical, and astrophysical data cannot exclude a deviation from the $1/R^2$ gravitational force law at a surprisingly large level. On the theoretical side, suggestions of a possible effective inverse-square-law violation have arisen both in the context of gravitation theory[3,6–9] and of particle theory.[10–16] Of particular interest is the suggestion by Scherk[10,11] in the context of supergravity unification schemes of a possible force of a long but finite range associated with a spin-1 member of a supermultiplet, and the suggestions by Moody and Wilczek,[15] and others,[16] that the long-sought pseudoscalar axion particle may have a mass such that it would mediate a force with a range on the order of a centimeter. These experimental and theoretical stimuli have led to many new experimental tests of the gravitational $1/R^2$ force law;[17–26] for a review see Ref. 27.

We published in 1980 a brief account[20] of a null experiment which tested the $1/R^2$ force law over a distance range of approximately 2 to 5 cm by probing the gravitational field inside a mass tube using a test mass suspended from a torsion balance. This experiment yielded results consistent with $1/R^2$ and, for reasonable parametrizations of an anomaly, inconsistent with the results of Long's experiment which tested a range from 5 to 30 cm. However, Long has suggested[28] that the anomaly he finds might arise from a vacuum polarization effect analogous to that which produces a logarithmic deviation from $1/R^2$ behavior at very short distances in the electric force between charges. Such an effect might not be observable in a null experiment such as ours, Long argues, because of the lack of a polarizing field in the region probed by the test mass.

We have conducted a second test of the $1/R^2$ force law which is not of null type in the sense objected to by Long, and which spans a distance range (5—105 cm) which includes the range tested by Long. In Sec. II of this paper we report this new experiment. In Sec. III we give additional details of our previously reported experiment and in Sec. IV we discuss the limits on inverse-square violation obtained from these experiments for various parametrizations of an anomaly.

II. THE 5—105-cm EXPERIMENT

A. Method

This experiment employs a torsion balance (Figs. 1 and 2) consisting of a uniform bar suspended at its midpoint. The instrument compares two torques: (a) the torque change produced by moving a 43-g cylindrical copper "near mass" m from a position 5 cm from one side of the bar, near its end, to a corresponding position on the opposite side of the bar, and (b) the simultaneous torque change produced by moving two 7.3-kg cylindrical copper "far masses" on carts from the darkened positions indicat-

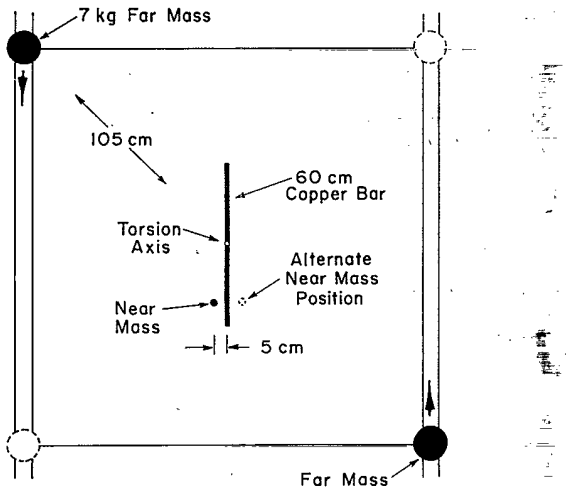

FIG. 1. Method of the 5—105-cm inverse-square-law test. The net torque change on the suspended bar is measured as the near and far masses move cyclically between the indicated solid and dashed positions. View is from above.

ed in Fig. 1 to the corresponding dashed positions, each 105 cm from the torsion axis of the balance.

The near-mass and far-mass values are chosen so that the net torque change in this operation should be nearly zero if the Newtonian force law is correct. Thus the test is a null experiment with respect to the net torque on the balance, with the attendant advantages of null experiments in regard to system nonlinearities, gain drifts, etc.; but is not a null experiment in the sense objected to by Long, in that different parts of the balance bar experience nonvanishing changing fields.

To eliminate the signal contribution from the poorly known mass distribution of the carts on which the far masses ride, as well as to eliminate other possible spurious signal components associated with the mass transport

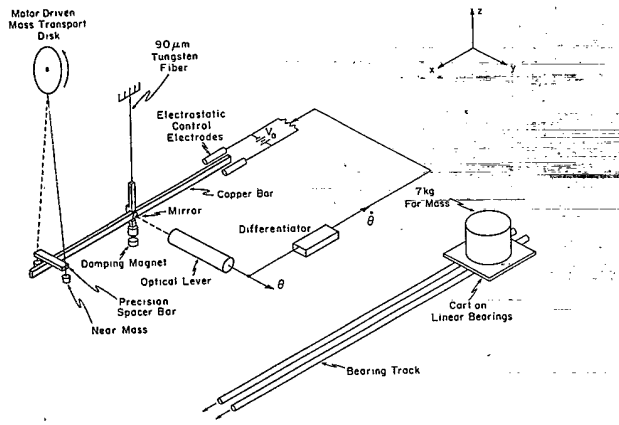

FIG. 2. Schematic of the 5—105-cm inverse-square-law test. Only one of the two far masses is shown. Also not shown are the vacuum housing, magnetic shielding, and thermal shielding which surround the torsion balance. The indicated coordinate system has its origin at the intersection of the torsion axis with the long axis of the bar.

such as systematic effects associated with contact closures, the experiment is repeated with the far masses removed from the carts and the 43-g near mass m replaced with a 3-g mass m' chosen to produce a torque canceling that due to the empty carts. The net torque signal from the run with unloaded carts is then subtracted from the net signal with loaded carts, yielding the approximately zero torque difference $\Delta N = N_{105} - N_5$ which would result from a cartless transport of the two far masses M at 105 cm (producing a torque change N_{105}), simultaneous with transport of a near mass equal to $m - m'$ at 5 cm (producing a torque change $-N_5$). An additional experimental run transporting only the near mass calibrates the ΔN measurement, and the ratio of torques $R_{\text{expt}} \equiv (N_{105}/N_5)_{\text{expt}}$ is thus determined. This ratio is then compared with the corresponding theoretical torque ratio calculated assuming a Newtonian force law: $R_{\text{Newton}} \equiv (N_{105}/N_5)_{\text{Newton}}$, yielding a measure of inverse-square-law violation:

$$\delta = \frac{R_{\text{expt}}}{R_{\text{Newton}}} - 1 .$$

B. Experimental detail

An important feature of this experiment is that the positions of the near and far attracting masses have symmetries which ensure that the measured torques are insensitive in first order to error in the position and/or angular orientation of the torsion balance. The features responsible for this are the following. (1) The far masses move on precision tracks along the sides of a square from one set of diagonally opposite corners to another, in a plane containing the torsion balance bar. Displacement of the torsion balance center from the center of this square in any direction by as much as 5 mm affects the torque change when the far masses are transported by less than 1 part in 10^4, and the torque change is similarly insensitive to a diamond-shaped distortion of the far-mass transport square, or to a rotation of the balance bar axis relative to the sides of the square. (2) The near mass is suspended in the horizontal plane containing the balance bar, at that position along its length at which the torque produced is a maximum (see Fig. 3), so that the torque is insensitive to error in near-mass position relative to the bar both vertically and along the bar axis direction. (3) The near mass is transported between opposite sides of the balance bar by the rotating disk indicated in Fig. 2, so that the distance between its two positions is precisely determined by the spacer bar indicated in the figure; the resulting torque change is sensitive to the lateral position of the balance bar only in second order. These features greatly ease the burden of metrology; the only critical geometrical quantities to be determined are the width of the near-mass spacer bar, the mean distance between diagonally opposite far-mass positions, and the geometrical parameters of the balance bar and the attracting masses.

The torsion balance beam was a 60-cm-long 523-g copper bar, suspended by a 20-cm long 90-μm diameter tungsten wire attached to the bar via a vertical copper

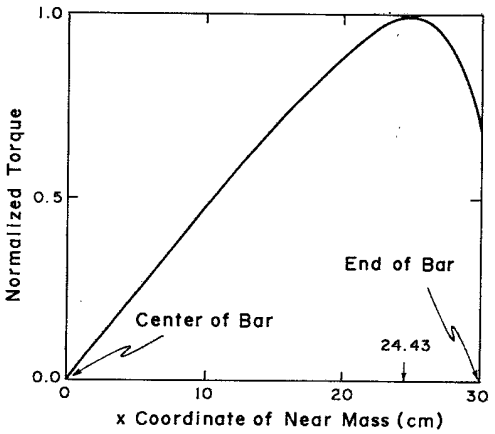

FIG. 3. Calculated torque on the balance bar as a function of the position of the near mass along its length. The torque value is insensitive to error in near-mass position when the near mass is located near the point $X=24.43$ where the torque is a maximum.

hanger element, as indicated in Fig. 2. The wire had a torsion constant of 50 dyn cm/rad; the balance had a natural torsional period of 350 sec with a Q of about 5000 corresponding to a damping time of about 77 h. The scale of the balance was made large, at some expense in sensitivity, to ease metrology tasks. The angular position of the balance was monitored with an optical lever: infrared light from a light-emitting diode (Texas Instruments TIES13) passed through a 100-μm hole in a mask, was made parallel by a lens, reflected from a mirror mounted on the torsion balance back through the same lens, and brought to a focus on a quadrant photodiode (Integrated Photomatrix, Inc. IPL30) in the same plane as the light-emitting diode. The differential output of opposite quadrants of the photodiode was amplified, passed through a low-pass filter, and recorded at 20-sec intervals by a DEC PDP 11/03 computer which monitored and controlled the experiment. In addition, the optical lever signal was differentiated, yielding a measure of the angular velocity of the balance. This velocity signal was fed to electrostatic control electrodes as indicated in Fig. 2, to damp torsional oscillations of the balance. The gain of this electronic damping servoloop was adjusted to give nearly critical damping of the torsional oscillation mode.

Damping of pendulum oscillation modes for the balance was provided by eddy currents induced in a copper cylinder on the bottom of the balance, by a stationary permanent magnet below. This damping reduced the Q of pendulum oscillation modes from over 10^6 to about 500, and significantly reduced the coupling of pendulum motion by nonlinear mechanisms into low frequency noise in the torsional mode. No significant degradation of the torsion mode Q was observed as a result of the pendulum mode damping.

The balance bar, vertical hanger, mirror, and damping cylinder, as well as the four attracting masses (m, m', and the two far masses), were all made of OFHC copper, machined using carefully cleaned tools to avoid introducing ferromagnetic impurities.

The torsion balance hung in a vacuum enclosure tailored to its shape, surrounded by magnetic and thermal shielding. The near and far attracting masses were external to this enclosure and shielding. An 8-l/sec ion pump maintained a vacuum of about 3×10^{-8} Torr within the vacuum enclosure. The entire apparatus operated in a thermally insulated 2.5-m deep steel-lined pit (Fig. 4), at a field site about 1/2 km from the nearest buildings or roads. The apparatus was controlled by an operator and computer in a trailer about 15 m from the pit. The periodic transport of the near mass and the recording of data was under the control of the computer, while the far masses on the carts were drawn along their tracks by a string and pulley system using small magnetically shielded motors under the control of the operator in the trailer.

Data were taken for cyclically alternating positions of the attracting masses as follows. A data cycle began with the transport of near and far masses between the solid and dashed positions indicated in Fig. 1; this transport required about 2 min. The balance was then allowed 13 min to reach a new equilibrium, and finally the optical level signal was recorded over a period of 2 min. The masses then were returned to their original positions, and data recorded after another 13-min wait.

A chart record of the signal associated with the uncompensated near mass torque, moving only the 43-g near mass, is shown in Fig. 5(a). A sample of the signal associated with moving simultaneously the near mass, far masses, and carts appears in Fig. 5(b); the nearly complete cancellation of torques, except during mass transits, is evident. (The variation from cycle to cycle in the amplitude of the signal excursion during mass transport is due to small variations in the relative transit durations for the near and far masses.) The torsion balance essentially measures the gradient of the gravitational field associated with the far mass; it is of interest to note its performance

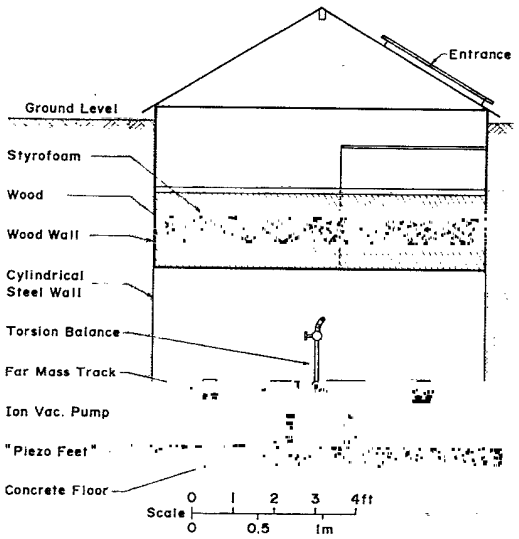

FIG. 4. Instrument chamber for the 5—105-cm experiment. The "far-mass" tracks, viewed here end on, are secured at their ends to the cylindrical steel walls of the chamber.

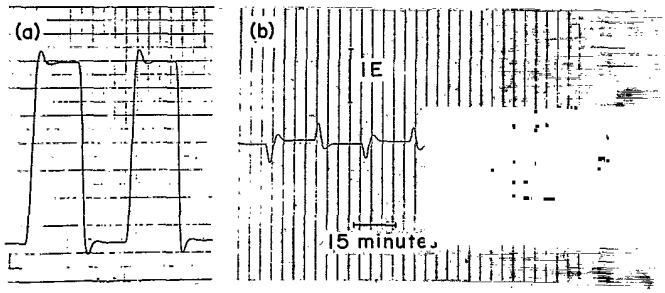

FIG. 5. Data samples from the 5—105-cm experiment; chart records of (a) the torque signal S_m resulting from transporting only the 43-g near mass m and (b) the signal S_{M+C+m} resulting from transporting simultaneously the near mass and the far masses on their carts. Indicated above is the signal amplitude corresponding to a field gradient of $1E$ ($=10^{-9}$ sec^{-2}).

as a gradiometer: the signal noise and drift in Fig. 5 may be compared with the indicated signal magnitude corresponding to a field gradient of $1E$ ($1E=10^{-9}$ cm sec^{-2}/cm). The instrument has a drift rate of less than $0.2E$/day, and a night-time equivalent noise level of less than $0.1E/\sqrt{\text{Hz}}$ at 0.001 Hz.

The magnitude of the torque on the balance due to either the far masses or the near mass alone was about 2×10^{-4} dyn cm, equal to the torque produced by a field gradient of $1.7E$. If unbalanced, this produces an angular deflection of 4×10^{-6} rad.

C. Data analysis: R_{expt}

Our results are based on two nights' runs, each involving 15 mass transports, or 7 round-trip transport cycles. In the first run, the near mass m was transported simultaneously with the far masses M on their carts C, yielding a mean optical lever signal difference for the two mass configurations: $S_{M+C+m}=(-0.1246\pm0.0015)$ V. The second run, the following night, transported the unloaded carts simultaneously with the small compensating near mass m', yielding a mean signal difference $S_{C+m'}=(-0.0135\pm0.0017)$ V. Short calibration runs each night, transporting only the near mass m, yielded $S_m=(6.496\pm0.004)$ V. This much larger signal includes a 0.7% correction for nonlinearity of the optical level response. This nonlinearity was determined in two ways, yielding consistent results: (1) by comparing the signal due to transporting each of the far masses separately with the signal due to transporting the far masses together and (2) by comparing the signals S_m and $S_{m'}$ due to transporting, respectively, only m and only m', where ideally $S_m/S_{m'}=m/m'$.

The distribution of torque signals for individual round-trip cycles in the two data runs is presented in Fig. 6.

The experimental ratio $R_{\text{expt}}=N_{105}/N_5$ may now be determined, where N_{105} is the torque change that would result from transport of the far masses without their carts and N_5 is the torque change which would result from the transport of a near mass equal to $m-m'$:

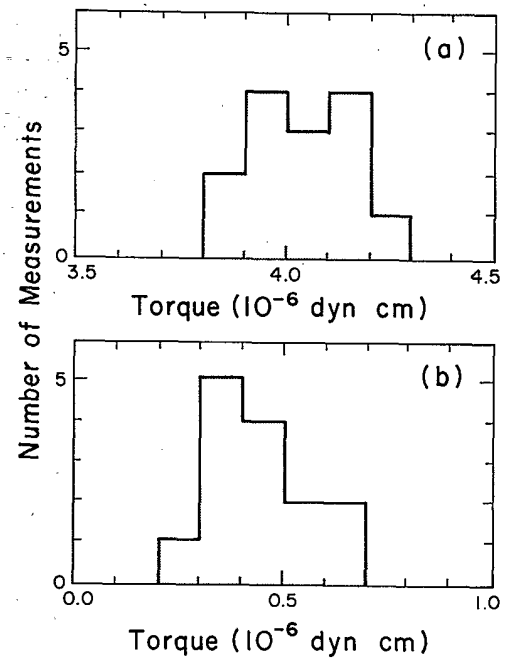

FIG. 6. Torque signals from individual mass transport cycles: (a) transporting far masses on their carts together with the near mass m and (b) transporting the unloaded carts, with the small compensating mass m'. The indicated torques are one half of the net torque change due to each mass transport.

$$R_{\text{expt}}\equiv1-\frac{m}{m-m'}\left[\frac{S_{M+C+m}-S_{C+m'}}{S_m}\right]$$

yielding $R_{\text{expt}}=1.018\,37\pm0.000\,37$.

Two points should be noted, which are both consequences of the fact that the two data runs, with and without masses on the carts, are each separately close to null experiments. First, R_{expt} is very insensitive to possible system gain variation between the two runs a day apart and second, the 0.7% nonlinearity correction to the calibration signal S_m changes R_{expt} by only 1.3×10^{-4}.

D. Calculations of R_{Newton} and δ

The value of $R=N_{105}/N_5$ expected assuming an inverse-square-force law was calculated as follows. First the expected torques N_{105} and N_5 were computed with a six-dimensional numerical integration, assuming a geometrically perfect balance bar of uniform density. The values of the relevant parameters for this calculation are indicated in Table I, along with the contributions of their uncertainties to the uncertainty in the computed values of N_{105} and N_5. Masses were determined by the Los Angeles County Department of Weights and Measures. The value of the mean radial positions of the far masses ($\bar{r}_{105}$) was computed from measurements of the distance between the rest positions of the far mass cylinders at the four corners of the square frame on which they are transported. This measurement was made with a long inside micrometer in the laboratory before assembly of the transport system in the instrument pit, and again after assem-

TABLE I. Parameters and associated torque uncertainties for calculated Newtonian torques, 5—105-cm experiment.

Parameter	Value (cgs)	$10^4\delta N_5/N_5$	$10^4\delta N_{105}/N_{105}$
Balance bar length	59.959±0.006	±0.22	±2.0
Balance bar height[a]	1.503±0.002	±0.24	<0.01
Balance bar width[a]	0.651±0.002	±0.12	<0.01
Width of near mass spacer[b]	9.5801±0.0008	±1.1	
x coordinate of near masses	24.41±0.10	+0−1	
Mean y coordinate of near masses	0.02±0.03	+1.2/−0.2	
z coordinate of near masses	−0.03±0.05	+0.4/−2.7	
x coordinate of bar center	−0.0065±0.004	±1.8	
Diameter of mass m	1.9333±0.0002	±0.02	
Height of mass m	1.6693±0.0020	±0.3	
Diameter of mass m'	0.7957±0.0005	<0.1	
Height of mass m'	0.6932±0.0010	<0.1	
Diameter of far masses	10.616±0.002	±0.01	
Height of far masses	9.195±0.005	±0.02	
Mean radial coordinate of far masses	105.016±0.008		±2.2
ΔX_M[c]	0±0.2		±0.2
ΔY_M[c]	0±0.2		±0.2
ΔZ_M[c]	0±0.3		±0.2
Mass of m	43.583±0.005	±1.3	
Mass of m'	3.0165±0.004	±1.0	
Mass of north far mass	7265.854±0.050		±0.05
Mass of south far mass	7266.470±0.050		±0.05
Mass of balance bar	523.1±0.1	———[d]	———[d]
Cumulative uncertainties		4.1	3.0

[a]Associated torque uncertainties here assume a perfectly uniform bar.
[b]Includes diameter (0.002 cm) of the "near-mass" suspension wire.
[c]ΔX_M, ΔY_M, and ΔZ_M represent deviations of "far-mass" positions from the corners of a pefectly aligned square.
[d]Uncertainty in bar mass does not contribute to uncertainty in the ratio R_{Newton} of near and far mass torques.

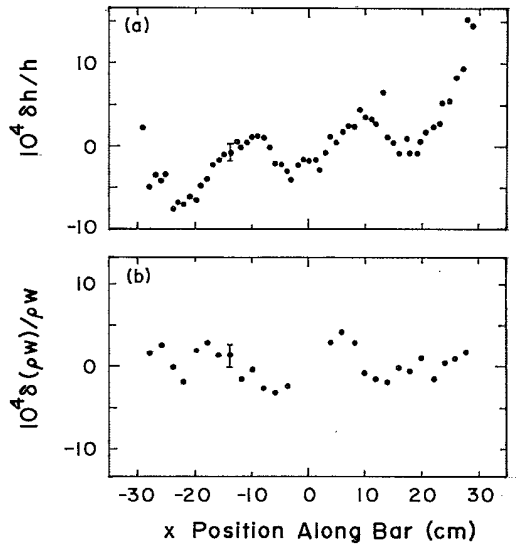

FIG. 7. Fractional variations in (a) the height h of the torsion balance bar along its length and (b) the mass thickness ρw of the bar, determined by a γ scan. A typical data point uncertainty is indicated in each plot.

bly in the pit just before taking data. The uncertainty in $\bar{r}_{105}$ includes a contribution due to uncertainty in the temperature of the micrometer during pit measurements.

The calculated torques in this experiment depend critically on measurement of deviation from uniformity of the balance bar, which was cut from $\frac{1}{4}$-in.-thick OFHC copper sheet stock. The variation in height h of the bar as a function of position along its length was measured with a micrometer, while the variation in the product of the thickness w of the bar and its density ρ was determined along its length by measuring the variation in transmission through the bar of γ radiation from a 30-mCi ^{137}Cs source. The latter measurement was made by sliding the copper bar in increments periodically back and forth in a guide between the collimated γ source and a NaI detector, while signal averaging the current output of

TABLE II. Corrections to calculated Newtonian torques due to bar nonuniformity, 5—105-cm experiment.

Origin of correction	$10^4\Delta N_5/N_5$	$10^4\Delta N_{105}/N_{105}$
Mirror and bar hanger	−0.04±0.2	−0.53±0.2
h variation along bar	5.64±1.0	1.03±0.5
ρw variation along bar	0.67±1.7	0.92±1.5

the detector over a total period of about 24 h.

The fractional variations $\delta h/h$ and $\delta(\rho w)/\rho w$ determined by the measurements are plotted as functions of position along the bar in Fig. 7. The resulting computed corrections to the torques N_{105} and N_5 due to far and near masses, respectively, are indicated in Table II, along with the small corrections due to the elements of the torsion balance other than the horizontal bar. With these corrections the computed value of R assuming an inverse square force law becomes $R_{\text{Newton}}=1.018\,25\pm0.000\,58$.

Comparing the experimental and computed Newtonian values for the ratio R, we obtain a measure of inverse-square violation:

$$\delta\equiv\frac{R_{\text{expt}}}{R_{\text{Newton}}}-1=(1.2\pm7)\times10^{-4}\,.$$

Table III summarizes the contributions to the uncertainty in δ, including limits on potential systematic errors discussed in the following section.

E. Sources of systematic error

1. Tilt effects. Small tilts of the floor on which our apparatus rests can produce in at least two ways a signal which simulates the signal due to a gravitational torque change: (a) Tilt causes the balance, which hangs always vertically, to change its position relative to the electrostatic control plates at the end of the balance bar, thus changing the electrostatic force applied at that point and producing a spurious torque on the balance and (b) tilt causes the image of the reflected light spot in the optical lever system to shift vertically on the quadrant photodetector, which can change the relative output of horizontally opposed quadrants of the detector, simulating a rotation of the balance. Floor tilt may be associated with the change in positions of the near and far masses, suggesting a potentially serious source of systematic error. The design of our experiment makes the tilt associated with mass transport exceedingly small, however. The near mass hangs from a transport mechanism which is mounted on a long aluminum channel fastened at its ends to opposite portions of the steel wall of the instrument pit. When the near mass is transported, the 10-cm shift in the position at which its weight is applied to this support channel produces a relative change in force transmitted to the steel pit walls of less than a tenth of the weight of the near mass, with negligible effect on floor tilt. The transport of a single far mass produces a much greater change in the floor loading, but the two masses moving together apply their weight with a symmetry which should produce no floor tilt at the location of the torsion balance if the ground is uniform.

TABLE III. Summary of contributions to final uncertainty in δ, 5—105-cm experiment.

Origin	Uncertainty in δ ($\times10^4$)
Geometrical parameters (assuming uniform bar)	4.8
Bar nonuniformity measurement	2.8
Mass values	1.6
Noise (microseismic and gravitational)	3.7
Magnetic effects	<0.5
Tilt effects	<0.5
Optical lever nonlinearity	0.4
Cumulative uncertainty	6.9

To put a limit on possible tilt effects, we first determined the tilt sensitivity of the instrument's torque signal by deliberately tilting the instrument by about one microradian in each orthogonal axis in turn, using piezoelectric elements under the three legs of the instrument's base (labeled "piezo feet" in Fig. 4), while monitoring the tilt with a two-axis tiltmeter. Second, the actual tilt of the instrument associated with transporting a single far mass was measured with the tiltmeter to be $(4\pm1)\times10^{-8}$ rad along the x axis and $(0.0\pm0.5)\times10^{-8}$ rad along the y axis. With the previously determined tilt sensitivity this tilt was found to imply a spurious torque signal which would correspond to a change in δ of $(1.1\pm0.3)\times10^{-4}$. Since the tilt associated with both far masses moving together should be far less than the tilt due to a single mass, the limit on the error in δ due to tilt was put conservatively at 0.5×10^{-4}.

2. Magnetic coupling. Care was taken to minimize the danger of magnetic couplings between the attracting masses and the torsion balance. The balance and masses were machined of OFHC high-purity copper with carefully cleaned tools, and the balance housing was almost entirely enclosed in two coaxial tubes of high permeability magnetic shielding. To test the sensitivity of the balance to magnetic effects, a data run was made transporting a single cart with its far mass replaced with a bar magnet oriented at a 45° angle to the vertical in the yz plane defined in Fig. 2. The effect of this magnet on the balance torque signal, after correcting for the gravitational effect of the magnet, mount, and cart, was equivalent to a change in δ of 15×10^{-4}. Since the magnetic moment of the magnet (1.5 J/T) was larger by a factor of 5×10^6 than the magnetic moment induced in one of the copper far mass cylinders by the Earth's magnetic field, and also many orders of magnitude larger than the magnetic moment of any ferromagnetic impurity in the attracting masses, the limit on error in δ due to magnetic couplings was put conservatively at 0.5×10^{-4}.

3. Experimenter bias. A concern in experiments of this sort, involving many small corrections and potential error sources, is the danger of unconsciously slackening analysis effort when the experimental result begins to look "right" in some sense, or of subconscious bias in selection of data when it is known which data will give a "reasonable" final result. To help protect ourselves against such dangers, the exact dimensions and mass of our "near mass" m were selected and kept secret by someone outside the experiment, so that we knew the mass of m to only 1% until we were prepared to report a result, regardless of its value, without further analysis. We then obtained and used the exact value of m for our calculation, and reported[27] the resulting value: $\delta=(-2\pm7)\times10^{-4}$. Since that report, further refinements of some parameters and the inclusion of the nonlinearity correction have, however, changed the value of δ to its present value of $+(1.2\pm7)\times10^{-4}$.

III. THE 2—5-cm EXPERIMENT

A. Cylinder null experiment

The 2—5-cm experiment approximates an ideal null experiment, in which any measured force on a test mass in the vicinity of a suitably symmetric source mass indicates an anomalous force law. For example, if gravity is exactly inverse square, a test mass inside a spherical mass shell or an infinitely long mass tube will not feel a changing force as the source mass moves. We measure the force on a test mass suspended inside a long hollow cylinder; the residual end effect in our cylinder of length $L=60$ cm and inside diameter $D=6$ cm is smaller by a factor of $(D/L)^2=10^{-2}$ than the force from one of the two half-cylinders that would result from slicing the cylinder along its axis.

A torsion balance (Fig. 8) similar to the balance used in the 5—105-cm experiment serves as the force transducer; the balance used in the 2—5-cm experiment differs by the addition of a test mass suspended from one end of the balance beam and a counterbalance at the opposite end. The test mass is centered vertically in the cylinder, and the cylinder moves laterally to bring the test mass alternately near opposite cylinder walls; the balanced forces include contributions from a range of distances, but are dominated by the mass centered in the near (2-cm distant) and far (5-cm distant) walls. The force measurement is repeated many times with different azimuthal orientations of the cylinder to average over inhomogeneities in the mass distribution, and with the cylinder removed from its cart to measure the gravitational effect of the cart alone. The cart measurement is subtracted from the cylinder measurement, and the difference is compared with a calculation of the end effect based on the inverse square law.

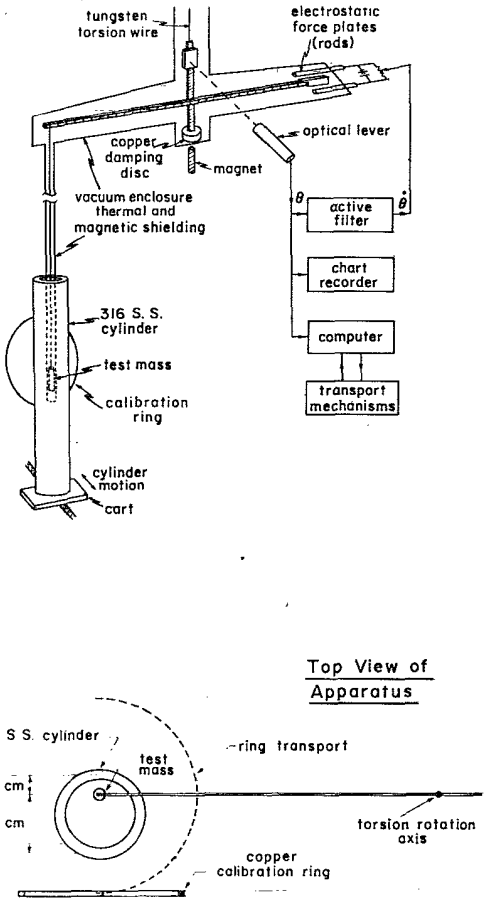

FIG. 8. The apparatus used for the 2—5-cm experiment. The top view shows the orientation of the test mass, cylinder, and calibration ring. The end-effect force, directed toward the near cylinder wall, is opposed by the force due to the ring. Cylinder and ring move cyclically between the positions shown and positions symmetrically opposite the test mass.

B. Experimental details and data collection

The design goal of the experiment was to compare the force between 2 and 5 cm with a precision of 1 part/10^5, which requires an acceleration sensitivity of 2×10^{-11} cm/sec^2. The 32-cm-long, 75-μm-diameter fiber supporting the 120-g balance assembly had a torsion constant of 13 dyn cm/rad; the required angular deflection sensitivity is 1×10^{-9} rad, or 2×10^{-8} cm displacement of the test mass. The torsional period was 400 sec and the amplitude damping time was 5 days. The vacuum enclosure, pump, magnetic shielding, optical lever, active electrostatic and passive magnetic damping were similar to the 5—105-cm experiment. An inner layer of thermal shielding consisted of a 1.8-cm-thick layer of fiberglass covering the vacuum plumbing along the length of the balance boom, and of two concentric copper tubes separated by a 0.6-mm air gap surrounding the test mass vacuum jacket. A styrofoam house with 20-cm walls and roof enclosed the apparatus, which was located in a basement laboratory.

The cylinder, of mass 10.44 kg and wall thickness 1 cm, was made of high-purity double-vacuum-melted, type-316 stainless steel. Its associated magnetic field at points about 1 cm from the surface of the tube was measured to be less than 5 nT. The test mass was a 20-g, 4.4-cm-long cylinder of high-purity copper, hanging 83 cm below the end of a torsion-balance boom of total length 60 cm, made of oxygen-free high-conductivity copper. Carefully cleaned tools were used to prevent the introduction of ferromagnetic impurities during machining of the balance components.

The radial component g_r of the gravitational field inside the cylinder (the end-effect field) may be written as a power expansion

$$g_r(x,\zeta)=\frac{GM}{RL}\{[\alpha^2-\tfrac{3}{4}\alpha^4(1+k^2)+\tfrac{5}{8}\alpha^6(1+k^2+k^4)]x+[-\tfrac{3}{4}\alpha^4+\tfrac{15}{8}\alpha^6(1+k^2)]x^3+(\tfrac{5}{8}\alpha^6)x^5$$
$$+[3\alpha^4-\tfrac{15}{2}\alpha^6(1+k^2)]x\zeta^2+(-\tfrac{15}{2}\alpha^6)x^3\zeta^2+(5\alpha^6)x\zeta^4+O(\alpha^8)\}\ ,$$

where R is the inner radius, k the ratio of outside radius to inside radius, M the cylinder mass, L the cylinder length, r and z, respectively, the radial and axial positions of a point inside the cylinder, $\alpha=2R/L$, $x=r/R$, and $\zeta=z/R$. The field is nearly linear in position along a diameter, even for positions far from the median plane. For a 1 part/10^5 measurement of the unbalanced field, we need measure only the relative motion of the cylinder to just 1 part/10^3, while the absolute position of the cylinder relative to the test mass need only be known to a few mm.

Calibration of the balance was accomplished with a 133-g copper ring of radius $R'=12.1$ cm located so that the test mass lay on the ring axis at the position $(z=R'/\sqrt{2})$ where the force due to the ring is a maximum and hence insensitive to the exact location of the test mass. The ring mass was chosen to produce a force on the test mass approximately equal to the end-effect force it calibrates.

The motions of the cylinder, calibration ring, and tilt compensating device (described below) were controlled by a PDP 11/03 computer, which also recorded signals. Data were collected late at night, when the laboratory was unattended. A 5-h sample of the optical lever horizontal axis output is shown in Fig. 9. The smaller periodic signal has a peak-to-peak amplitude of 4×10^{-7} rad; each transition results from the simultaneous motion of the cylinder by 3.43 cm and of the ring from one side of the test mass to the other. The motions are phased so the end effect balances the force from the ring; the two large calibration peaks result from motion of the ring alone. The prominent drift is due to temperature-correlated unwinding of the torsion fiber.

C. Data analysis

The torque measurements collected over a 3-week span are presented in Fig. 10. Figure 10(a) shows the torque change $N_\Sigma=N_{\rm cyl}+N_{\rm cart}+N_{\rm ring}$ due to 132 round-trip transits of the cylinder, its cart, and the calibration ring; Fig. 10(b) shows the torque change $N_{\rm cart}$, due to 48 round-trip transits of the cart alone.

The calibration of the torsion balance response was based on a Newtonian calculation of the torque due to the ring, taking $G=6.67\times10^{-8}$ dyn cm^2 g^{-2}. Since the calibration was of a small "end-effect" correction to a basically null experiment, errors in the calibration due to possible deviation from an inverse-square law would have only a second-order and hence negligible effect on the basic inverse-square-law test.

The cylinder data are from runs with eight equally spaced azimuthal orientations; results for different orientations are presented in Fig. 11. With equal weight given to each angular position, we find the average net torques N_Σ and $N_{\rm cart}$ listed in Table IV. The uncertainties indicated in Fig. 11 and associated with N_Σ and $N_{\rm cart}$ in Table IV are statistical only, reflecting the random variations in torsion balance signal associated with instrument

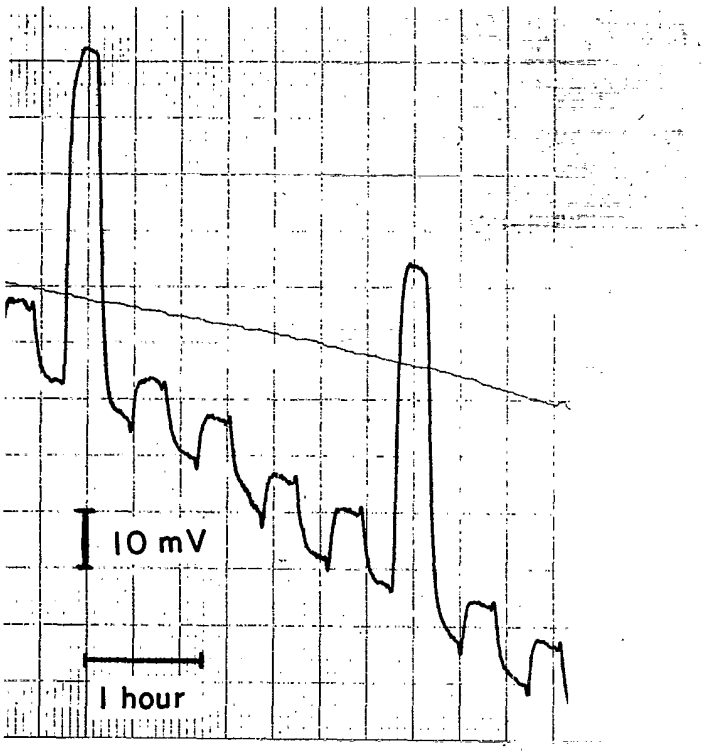

FIG. 9. Five-hour segment of the torque signal from the 2—5-cm experiment. The small peaks are associated with the simultaneous transport of the ring and the cylinder on its cart; the large peaks are associated with the transport of the ring alone.

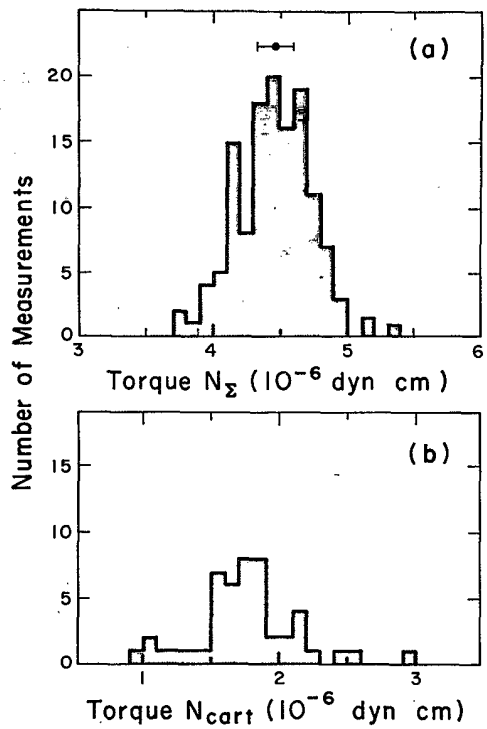

FIG. 10. (a) Distribution of 132 measurements of N_Σ, the torque change on the balance due to the simultaneous transport of the cylinder, cart, and ring. The Newtonian prediction is indicated above. (b) Distribution of 48 measurements of $N_{\rm cart}$, the torque change due to motion of the cart alone.

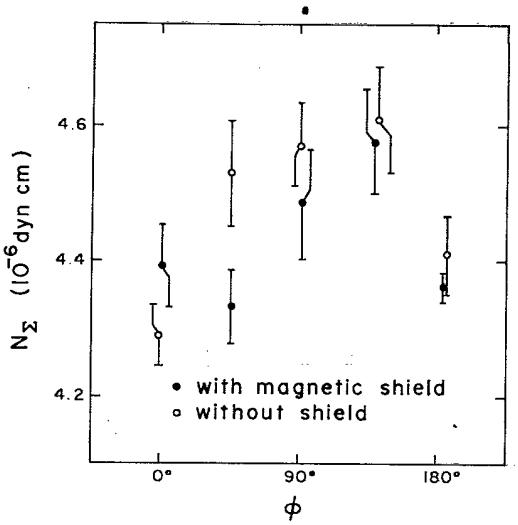

FIG. 11. Measured N_Σ with and without magnetic shielding surrounding the test mass. The data with shield are from the same measurements represented in Fig. 10.

noise, seismic noise, and torques due to gravitational field variations not associated with the moving ring and cylinder. These noise types are not easily distinguished in our experiment.

D. Comparison of measurements and the prediction of Newton's law

The components of the Newtonian prediction of the torque associated with motion of the cylinder and ring are listed in Table V. The calculation for the cylinder—test-mass interaction (end effect) assumes a perfectly symmetric and homogeneous cylinder, and includes a correction due to the test mass not being concentrated at a point. The torque due to the cylinder and ring interacting with balance components other than the test mass is much smaller than the end effect and does not significantly affect the null nature of the experiment. The ring-balance interaction includes a significant correction for the hangers which suspend the ring (total mass 3 g).

To correct for nonuniformities, the cylinder geometry and homogeneity must be measured to high precision, especially near the center. Some deviations from ideal symmetry, such as nonconcentric inside diameter (ID) and outside diameter (OD), a bowed cylinder axis, and a tilted ID axis have negligible effect on the force measurements. Azimuthal perturbations, such as an elliptic cross section of the cylinder wall, produce a measurable effect, but are averaged out by successive force measurements conducted at different azimuthal orientations. Variations of homogeneity and geometry along the cylinder axis enter in first order, and their effect is not reduced by azimuthal averaging.

TABLE IV. Measurements used to determine $N_{r+\mathrm{cyl}}$(expt), the experimentally determined torque change due to the ring and cylinder movement in the 2—5-cm experiment.

Interaction	Measured torque (10^{-6}dyn cm)
Cylinder + ring + cart (N_Σ)	4.49±0.03
Cart (N_{cart})	+ 1.74±0.05
Tilt effect	−0.04±0.03
Magnetic coupling[a]	0.00±0.06
Thermal effects	0.00±0.002
Nonlinearity	0.00±0.01
$N_{r+\mathrm{cyl}}$(expt)[b]	2.79±0.09

[a]Limited inferred indirectly from differential shielding tests.
[b]N_Σ minus remaining entries in table.

TABLE V. Newtonian calculation of $N_{r+\mathrm{cyl}}$(Newton), the torque due to (cylinder + ring) on (test mass + balance) in the 2—5-cm experiment. The torque due to the cart is not included.

Interaction	Torque contribution (10^{-6} dyn cm)
Cylinder—test mass	−25.83±0.01
Cylinder-balance	0.10±0.08
Ring—test mass	28.54±0.03
Ring-balance	−0.02±0.01
Cylinder nonuniformity correction	−0.02±0.06
Total $N_{r+\mathrm{cyl}}$(Newton)	2.77±0.11

We measured the cylinder OD, ID, and wall thickness along eight equally spaced axial lines, using a commercial differential gauging instrument with 0.1-μm resolution. Along the critical central 20 cm, measured wall thickness variation agreed within 0.5 μm with diameter difference variation.

Internal bubbles and other inhomogeneities were probed with γ rays from a 30-mCi ^{137}Cs source. The collimated source and a NaI scintillation detector straddled the cylinder wall, the source on the inside and the detector on the outside, each held stationary; the cylinder, mounted horizontally on a cart riding on precision steel rails, moved through its length every 20 sec for 4000 transits. Synchronous averaging of the photomultiplier current reduced the uncertainty due to counting statistics to 0.13 μm equivalent variation in wall thickness. Lead shielding around the source and detector was required to eliminate spurious fluctuations due to scattering by cart components. Scattering end effects limited the region of reliable measurements to the central region. The sensitivity of this γ scan to mass thickness variation was calibrated by 50-μm-thick strips of stainless-steel shim taped to the outside of the cylinder near each end.

Figure 12 shows the azimuthal average of eight γ scans along with the average of the gauge head wall thickness scans. Both curves are adjusted for wall thickness variation $\delta t=0$ at the center. The curves match well in the central 20 cm, and disagree by 7 μm near one end. The effect on the force measurements resulting from deviations from symmetry were calculated twice—first from the ID and OD measurements under the assumption of perfect homogeneity, and second from the γ-ray probe, under the assumption that the γ attenuation is proportional to integrated wall thickness (the force on the test mass is insensitive to the precise location of the nonhomo-

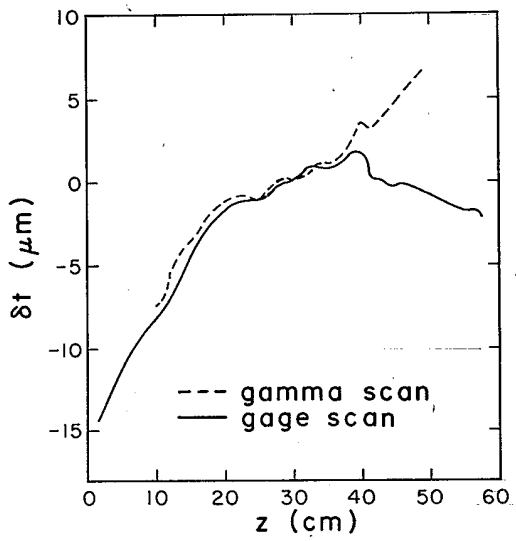

FIG. 12. Cylinder wall thickness variations along the cylinder axis, averaged over azimuthal orientation. The gauge scan measures the geometric wall thickness; the γ scan measures the effective wall thickness determined by the integrated mass distribution. The curves are adjusted to $\delta t=0$ at $z=30$ cm.

geneity within the cylinder wall).

The resulting correction is listed in Table V; the geometry measurement is more precise, but the γ probe is more direct. The value used for the contribution to the end effect due to deviations from symmetry of the cylinder is the unweighted average of the two estimates, with an uncertainty equal to their difference.

The bottom line of Table IV, which includes corrections discussed below, subtracted from the bottom line of Table V is a measure of any deviation from Newton's law:

$$\Delta=N_{r+\text{cyl}}(\text{expt})-N_{r+\text{cyl}}(\text{Newton}) ,$$

where $N_{r+\text{cyl}}$ represents the combined net torque change on the test mass and balance associated with the ring and cylinder movement. We find $\Delta=(+0.02\pm0.15)\times10^{-6}$ dyn cm.

E. Sources of systematic error

1. Magnetic effects

Possible magnetic forces directly associated with the cylinder that act on the test mass and, less strongly, on other balance components could be (1) a permanent dipole magnetic moment in the cylinder interacting with the balance through diamagnetism or ferromagnetic impurities in the balance, (2) a permanent dipole in the torsion balance interacting with the cylinder paramagnetically or through ferromagnetic impurities embedded in the cylinder wall, and (3) distortion of external magnetic fields caused by the magnetic permeability of the cylinder. Magnetic forces associated with the cylinder motion but not due to the cylinder itself can come from (4) fields generated by the transport motors or other moving magnetized parts of the mechanisms used to drive the cylinder and calibrating ring and (5) fields due to ferromagnetic impurities in the ring.

In cases (1) and (2), a permanent magnetic moment generates a field B which interacts with induced magnetization to exert a force on the test mass proportional to $B\nabla B$. Magnetometer measurements indicate that without the magnetic shielding the maximum value of $B\nabla B$ near the test mass is 3×10^{-9} G^2/cm; the resulting maximum force on the unshielded diamagnetic copper test mass would be on the order of 5×10^{-15} dyn, negligible compared to the target sensitivity of 4×10^{-10} dyn. This effect is proportional to B^2, and is further reduced by magnetic shielding of high permeability metal which surrounds the entire balance housing.

The external field coupling (3) is negligible on two counts. First, a uniform external field perpendicular to the cylinder axis (as from Earth's field) is modified by the stainless-steel cylinder's susceptibility by less than $\chi\approx3\times10^{-3}$. Second, the field inside is still uniform, and can thus have no effect when the cylinder is moved. Motors were magnetically shielded and remotely located to reduce coupling (4); the drive force for the cylinder and ring was provided by strings. When possible, nonmagnetic materials were used for moving parts; one exception is steel bearings in the cylinder cart. Magnetic effects associated with the ring are small compared to the cylinder since the ring is smaller, less magnetic, and farther from the test mass than the cylinder.

A test for magnetic effects was made by repeating data runs with five cylinder azimuthal positions after removing the magnetic shielding surrounding the test mass; results are shown in Fig. 11, compared with the results with shielding. The mean torque computed for the data without magnetic shielding is in good agreement with the torque for data with the shield, differing by $(3\pm4)\times10^{-8}$ dyn cm. A separate test of the shield with a magnetometer showed it suppressed low-level magnetic fields by a factor of 4. A reasonable upper limit on the torque associated with magnetic fields when the shield is in place is then $(3+4)\times10^{-8}/(4-1)=2.3\times10^{-8}$ dyn cm. We assigned a more conservative uncertainty associated with magnetic coupling of 6×10^{-8} dyn cm.

2. Correlated tilt

The cylinder cart travels on a shelf at the side of the 0.5-ton concrete block which supports the torsion balance; when the cylinder moves its standard distance of 3.4 cm, the block tilts 1.0×10^{-7} rad. The balance support point shifts slightly while the balance remains plumb, resulting in a relative motion between the test mass and the nearby vacuum wall, and between the counterbalance and electrostatic control electrodes flanking the counterbalance. These position changes in nonuniform electric fields produce force changes at the ends of the balance causing a spurious tilt-dependent angular deflection. The tilt generated by the cylinder motion generated a 2×10^{-8} rad deflection of the balance, an order of magnitude greater than the design sensitivity.

A compensating torque was applied to the block during data collection which reduced the 10^{-7} rad tilt by a factor

of 8. Two wires under tension and fixed to the block transmitted the compensating torque, which was provided by a remotely located motor-driven apparatus designed to keep the sum of the tensions constant. The effectiveness of this scheme was monitored in three ways: by a vertical tiltmeter on top of the concrete block, by gage heads measuring the displacement of the block relative to the floor, and by the vertical axis output of the optical lever. The consistency of the three measurements allowed a precise determination of the residual tilt effect, listed in Table IV.

3. *Other systematic effects*

A temperature difference ΔT in the residual gas on opposite sides of the test mass, area A, causes a net force $\Delta F = AP_0\Delta T/T$. At the working pressure of $P_0 = 3\times10^{-7}$ Torr, the maximum tolerable temperature difference excursion correlated with the cylinder motion (as may be caused by one side of the cylinder hotter than the other) is 4×10^{-5} C. Reducing the residual gas pressure would help only down to 4×10^{-9} Torr; at lower pressure radiation pressure dominates. The effectiveness of the double heat shield around the test mass was measured by differentially heating the outside of the shield to produce a temperature gradient 1000 times larger than occurs in normal operation. We conclude that thermal gradient effects contribute the negligible amount to systematic error listed in Table IV.

The linearity of the response of the torsion balance was checked by reversing the phase of the motion of the ring relative to the cylinder, so the forces on the test mass add rather than cancel. The cylinder and ring were also moved individually; the sum effect equals the effect of their simultaneous motion to high precision, indicating that nonlinearities contribute the small amount of uncertainty listed in Table IV.

Experimenter bias was minimized by making a final determination of the number for $N_{r+\text{cyl}}$(expt), including correction for the tilt effect, before calculating the prediction of Newton's law. Then the cylinder geometry was measured, and $N_{r+\text{cyl}}$(Newton) was calculated independently by two experimenters.

IV. DISCUSSION OF RESULTS

Deviation from an inverse-square distance dependence of the gravitational force is conveniently expressed in terms of an effective distance dependence of the gravitational constant G as it appears in the force law:

$$F = \frac{G(r)Mm}{r^2} . \tag{1}$$

The form for inverse-square deviation expected in theories involving the exchange of a finite-mass particle coupling to mass is given in terms of an interaction potential energy by

$$V = \frac{-G_\infty Mm}{r}(1+\alpha e^{-r/\lambda}) \tag{2}$$

which adds to the normal gravitational interaction a Yukawa term characterized by a strength α and range λ. In general such a Yukawa term should be attractive ($\alpha>0$) for an exchanged particle of even spin, and repulsive ($\alpha<0$) for odd spin. For this form of the potential, $G(r)$ appearing in the force equation (1) takes the form

$$G(r) = G_\infty[1+\alpha(1+r/\lambda)e^{-r/\lambda}] . \tag{3}$$

In Fig. 13 we present the constraints on the parameters α and λ of Eq. (2) which are determined by the two experiments of this work at a 1σ level, along with the locus of (α,λ) values consistent with Long's published result[1] at a 1σ level. It may be seen that each of our experiments puts

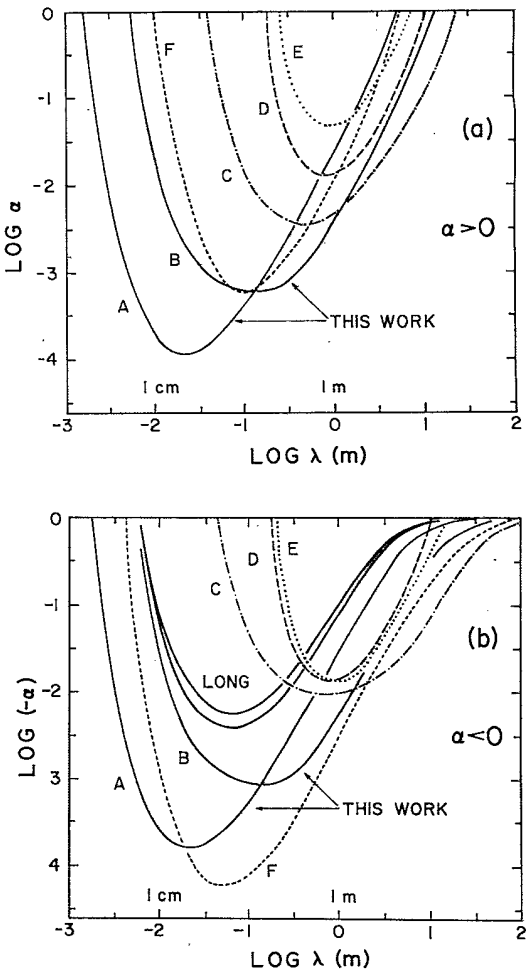

FIG. 13. Experimental constraints on the parameters (α,λ) of a Yukawa component of the gravitational force [Eq. (2)], for (a) positive α and (b) negative α. The shaded region marked "Long" represents 1σ limits for (α,λ) values consistent with Long's published results (Ref. 1). The regions above the other curves are excluded at a 1σ level by the following experiments. Curves A and B result, respectively, from our 2–5-cm and 5–105-cm experiments. Curve C is implied by the results of Panov and Frontov (Ref. 18). Curve D is from Ogawa, Tsubano, and Hirakawa (Ref. 22). Curve E is from Chan, Moody, and Paik (Ref. 23). Curve F is from Chen, Cook, and Metherell (Ref. 26).

a constraint on α which is inconsistent with Long's result for all values of λ.

Also plotted in Fig. 13 are 1σ level constraints on α and λ obtained from other experiments. Curves D, E, and F are taken, respectively, from the papers of Ogawa, Tsubono, and Hirakawa,[22] Chan, Moody, and Paik,[23] and Chen, Cook, and Metherell.[26] Curve C is our calculation of the constraint implied by the experiment of Panov and Frontov,[18] based on their published comparison of measured torques on a torsion balance produced by masses at various distances. [This comparison is presented by Panov and Frontov as the ratios of effective values of G at various distances; however the effective G so defined is not the $G(r)$ of Eq. (3), since their instrument, like ours, measures the gradient of a gravitational field. The curves C of Fig. 13 are based on our computation of torque ratios assuming the force law of Eq. (3).]

An alternative parametrization which is useful in expressing deviation from an inverse-square force involves a parameter ϵ which, for small values, may be defined in several ways which are equivalent to first order in ϵ:

$$\epsilon = r\frac{d}{dr}\ln G(r) , \tag{4a}$$

$$G(r) = G_0[1+\epsilon \ln r(\text{cm})] , \tag{4b}$$

$$F \propto r^{-2+\epsilon} , \tag{4c}$$

$$V \propto r^{-1+\epsilon} . \tag{4d}$$

Expressions (4b)—(4d) are taken to apply over limited ranges of r.

Comparing our experimental results with torques computed using Eq. (4b) we obtain the following values for ϵ:

$$\epsilon = (1\pm 7)\times 10^{-5} \quad (2\text{—}5\text{cm exp}) ,$$

$$\epsilon = (5\pm 27)\times 10^{-5} \quad (5\text{—}105\text{—cm exp}) .$$

The value for this parameter published by Long corresponds to $\epsilon_{\text{Long}} = (200\pm 40)\times 10^{-5}$, inconsistent with the result of both of our experiments.

In summary, neither of our experiments gives evidence for inverse-square violation; together they put strong limits on violation for mass separation between about 1 cm and 1 m.

ACKNOWLEDGMENTS

John Pellam made valuable suggestions in the early part of this work. We are grateful to many able student assistants in this work, especially to Robin Hanson and Tim Armstrong. We gratefully acknowledge encouragement and helpful suggestions from R. Drever, D. Long, J. Faller, H. Preston, F. Reines, and J. Weber. This work was supported by the National Science Foundation.

*Current address: Joint Institute for Laboratory Astrophysics, Boulder, Colorado 80309.

†Current address: Department of Physics, California Institute of Technology, Pasadena, California 91125.

[1]D. R. Long, Nature **260**, 417 (1976).

[2]F. D. Stacey and G. J. Tuck, Nature **292**, 230 (1981).

[3]Y. Fujii, Nature Phys. Sci. **234**, 5 (1971).

[4]D. R. Long, Phys. Rev. D **9**, 850 (1974).

[5]D. R. Mikkelsen and M. J. Newman, Phys. Rev. D **16**, 919 (1977).

[6]Y. Fujii, Ann. Phys. (N.Y.) **69**, 494 (1972).

[7]J. O'Hanlon, Phys. Rev. Lett. **29**, 137 (1972).

[8]R. V. Wagoner, Phys. Rev. D **1**, 3209 (1970).

[9]G. W. Gibbons and B. F. Whiting, Nature **291**, 636 (1981).

[10]J. Scherk, Phys. Lett. **88B**, 265 (1979).

[11]J. Scherk, in *Unification of the Fundamental Particle Interactions,* edited by S. Ferrara *et al.* (Plenum, New York, 1981), p. 381.

[12]J. R. Primack and M. A. Sher, Nature **288**, 680 (1980).

[13]G. Feinberg and J. Sucher, Phys. Rev. D **20**, 1717 (1979).

[14]L. B. Okun', Zh. Eksp. Teor. Fiz. **52**, 694 (1980) [Sov. Phys.JETP **52**, 351 (1980)].

[15]J. Moody and F. Wilczek, Phys. Rev. D **30**, 130 (1984).

[16]J. E. Kim, Phys. Rev. Lett. **43**, 103 (1979).

[17]H. T. Yu *et al.*, Phys. Rev. D **20**, 1813 (1979).

[18]V. I. Panov and V. N. Frontov, Zh. Eksp. Teor. Fiz. **77**, 1701 (1979) [Sov. Phys. JETP **50**, 852, (1979)].

[19]H. Hirakawa, D. Tsubono, and K. Oide, Nature **283**, 184 (1980).

[20]R. Spero, J. K. Hoskins, R. Newman, J. Pellam, and J. Schultz, Phys. Rev. Lett. **44**, 1645 (1980).

[21]F. D. Stacey *et al.*, Phys. Rev. D **23**, 1683 (1981).

[22]Y. Ogawa, D. Tsubono, and H. Hirakawa, Phys. Rev. D **26**, 729 (1982).

[23]H. A. Chan, M. V. Moody, and H. J. Paik, Phys. Rev. Lett. **49**, 1745 (1982).

[24]A. P. Mills, Jr., Gen. Relativ. Gravit. **11**, 1 (1979).

[25]W. C. Oelfke, in *Precision Measurement and Fundamental Constants II,* edited by B. N. Taylor and W. D. Phillips (National Bureau of Standards Special Publication No. 617).

[26]Y. T. Chen, Alan H. Cook, and A. J. F. Metherell, Proc. R. Soc. London **A394**, 47 (1984).

[27]R. D. Newman, in *Proceedings of the Third Marcel Grossman Meeting on General Relativity,* edited by Hu Ning (North-Holland, Amsterdam, 1983).

[28]D. R. Long, Nuovo Cimento **55B**, 252 (1980).